Journal of Molecular Graphics and Modelling 52 (2014) 20–29

Contents lists available at ScienceDirect

Journal of Molecular Graphics and Modelling

journal homepage: www.elsevier.com/locate/JMGM

Mechanistic insights into the catalytic reaction of plant allene oxide synthase (pAOS) via QM and QM/MM calculations

Tuanjai Somboon[a], Jun Ochiai[b], Witcha Treesuwan[c], M. Paul Gleeson[a], Supa Hannongbua[a,d,*], Seiji Mori[b,e,*]

[a] Department of Chemistry, Faculty of Science, Kasetsart University, Chatuchak, Bangkok 10900, Thailand
[b] Faculty of Science, Ibaraki University, Ibaraki 310-8512, Japan
[c] Institute of Food Research and Product Development, Kasetsart University, Chatuchak, Bangkok 10900, Thailand
[d] Center of Nanotechnology KU, Kasetsart University, Chatuchak, Bangkok 10900 Thailand
[e] Frontier Research Center for Applied Atomic Sciences, Ibaraki University, Tokai, Ibaraki 319-1106, Japan

ARTICLE INFO

Article history:
Accepted 30 May 2014
Available online 12 June 2014

Keywords:
Cytochrome P450
Allene oxide synthase
AOS
QM/MM calculations
QM cluster calculation
DFT calculations

ABSTRACT

QM cluster and QM/MM protein models have been employed to understand aspects of the reaction mechanism of plant allene oxide synthase (pAOS). In this study we have investigated two reaction mechanisms for pAOS. The standard pAOS mechanism was contrasted with an alternative involving an additional active site molecule which has been shown to facilitate proton coupled electron transfer (PCET) in related systems. Firstly, we found that the results from QM/MM protein model are comparable with those from the QM cluster model, presumably due to the large active site used. Furthermore, the results from the QM cluster model show that the Fe^{III} and Fe^{IV} pathways for the standard mechanism have similar energetic and structural properties, indicating that the reaction mechanism may well proceed via both pathways. However, while the PCET process is facilitated by an additional active site bound water in other related families, in pAOS it is not, suggesting this type of process is not general to all closely related family members.

© 2014 Elsevier Inc. All rights reserved.

1. Introduction

Cytochrome P450 enzymes (CYP or P450s) are a large family of heme-containing enzymes. They are important enzymes involved in the metabolic transformation of endogenous and exogenous substances to either chemical precursors or to convert exogenous substances, such as drug, to hydrophilic chemicals that are more easily excreted from the body [1,2]. P450s represent a family of enzymes that catalyze the same reactions with a wide variety of substrates [3,4]. The family is responsible for catalyzing the majority of monoxygenase reactions. These P450 mediated reactions are carried out by incorporating one atom of oxygen into the substrates and the other oxygen atom is converted to water [5]. Furthermore, P450s also function in the biosynthesis of steroid hormones and signaling molecules [6–8], xenobiotic metabolism [9,10] and fatty acid hydroxylase [11,12]. Bacterial P450 are also of interest, being used in a variety of biotechnology applications [13,14]. In addition, plant cytochrome P450 has also been investigated from a plant protection and pharmacological perspective [15–17]. Plant allene oxide synthase (plant AOS) is a member of the CYP74A subfamily, which does not require O_2 or NADPH to catalyze reactions as found in typical P450 members [18]. Instead of catalyzing monooxygenation reactions, all members in this subfamily rearrange hydroperoxide fatty acids into new forms by using various biochemical transformations with very high catalytic efficiency [19–21]. These proteins are currently of major interest academically as the biochemical processes are not fully understood. Thus, insights into their reactivity from structural, biochemical and computational studies are of considerable interest to help improve our general understanding of this protein.

AOS rearranges fatty acid hydroperoxides into different precursors, including allene oxide, in plants, corals and starfish oocytes [22,23]. Allene oxides are further transformed into jasmonates (S1), which are a family of plant hormones. Jasmonates have high structural similarity to several prostaglandins which bear a cyclopentane ring. In addition, jasmonates and prostaglandins are important signaling molecules in plants and animals, respectively [24]. A number of X-ray structures on AOS have been published.

* Corresponding authors at: Faculty of Science, Ibaraki University, Mito, Ibaraki 310-8512, Japan, and Department of Chemistry, Faculty of Science, Kasetsart University, Bangkhen, Bangkok 10900 Thailand.
E-mail addresses: fscisph@ku.ac.th (S. Hannongbua), smori@mx.ibaraki.ac.jp (S. Mori).

http://dx.doi.org/10.1016/j.jmgm.2014.05.012
1093-3263/© 2014 Elsevier Inc. All rights reserved.

The structure of coral AOS shows that the active site contains a tyrosine (Tyr) ligated to Fe-heme and histidine (His) and threonine (Thr) are proximal to the substrate building site [25,26]. In contrast, plant AOS [23,27], a member of CYP family, contains cysteine (Cys) ligated to Fe-heme and the proximal residues close to the substrate building site are asparagine (Asn) and phenylalanine (Phe). However, it has been shown that the substrate of coral AOS is 8(*R*)-hydroperoxyeicosatetraenoic (8(*R*)-HPETE) acid while for plant AOS, also known as CYP74, the substrate is 13(*S*)-hydroperoxyoctadecatrienoic (13(*S*)-HPOT) acid, leading to allene oxide as shown in S2 [19,26].

Computational calculations have been applied to elucidate crucial enzymatic reactions [28–30]. The mechanism of P450 enzymes, with oxidation mechanisms and inhibition has received particular attention [30–36]. Plant AOS and related atypical P450s in the prostaglandin H_2 to prostacyclin pathway have also been studied extensively. Cho et al. reported a combined QM/MM study on the plant AOS reaction mechanism [37]. They found that Fe^{III} and Fe^{IV} mechanism were comparable, with the rate determining step of the O—O bond breaking equals to 19.9 kcal/mol. Yanai and Mori have investigated the isomerization of prostaglandin H_2 to prostacyclin with QM cluster model. It is found that the isomerization catalyzed by a related P450 protein proceeds preferentially (1.3 kcal/mol) via a proton-coupled electron transfer (PCET) mechanism due to its lower activation energy [38]. QM/MM simulations on the P450 BM3 catalytic mechanism have been studied [39]. The results show that a crystal water molecule plays a role as a catalyst and decrease the activation barrier by about 2 kcal/mol and reaction energy by 3–4 kcal/mol. In addition, role of active site water molecules has been experimentally studied [40]. The crystal structures show that three water molecules occupy the active site, forming hydrogen bonds with the distal dioxygen molecule. These active site water molecules were proposed to participate in the proton transfer and oxygen cleavage in cytochrome P450 158A2 by stabilizing a water pathway for proton transfer. Recently, a computational investigation on the proton/electron transfer reaction between cysteine residue and tyrosinyl radical has revealed that an inserted water molecule mediates a doubled proton coupled electron transfer (dPCET) mechanism [41]. The reaction mechanism of coral AOS has also been computationally investigated using a DFT-chemical cluster model [42,43]. Bushnell et al. showed that the coral AOS mechanism proceeds through Fe-oxo species. The proposed reaction mechanism begins when the 8(*R*)-HPETE acid binds to the Fe(III)-heme and homolytic O—O bond cleavage occurs leading to oxygen radical with a compound II (Cpd II) intermediate complex, which is found that oxygen can be doubly bound to Fe(IV)-heme. Then the reaction further undergoes the epoxide formation with the electron transfer onto Cpd II and the last step is PCET from the substrate carbon adjacent to the epoxide moiety to his residue forming C=C double bond onto the substrate. On the contrary to the typical P450s, it was proposed that plant AOS is unusual among P450s in that its reaction mechanism occurs without passing the Fe-oxo species as found in thromboxane and prostacyclin biosynthase from prostaglandin H_2 [38,44–46].

In this study, we investigate whether the PCET mechanism in pAOS is also facilitated by an additional active site water molecule. We apply QM cluster and QM/MM protein models to further study these aspects of AOS reactivity. Due to the fact that the most suitable starting structure (PDB code: 3DSI [23]) lacked the expected Fe—O bond and the fact that the heme was in a sub-optimal conformation (S4), we investigated how these factors affect the mechanism. We were also interested in investigating both a QM cluster model (in the absence of the environment), as well as the effect of a critical phenylalanine (Phe) residue QM as proposed by Lee et al. [23]. In addition, we also assess the energetic differences Fe^{III} and Fe^{IV} have on the reaction mechanism [47,48]. The proposed reaction mechanisms of plant AOS (Fe^{III}) are shown in Schemes 1 and 2. Finally, we have included an additional water molecule to study the water facilitated PCET mechanism [39,40].

2. Methodology

2.1. Protein preparation

The crystal structure of AOS was downloaded from RCSB protein data bank (PDB Code: 3DSI [23]). Although the 3DSI structure is of high resolution (1.8 Å), and contains a bound ligand very similar to the substrate under investigation here, additional modifications to the structure were needed before QM/MM calculations were undertaken. The substrate in AOS protein structure lacks the peroxide oxygen and this was added in a conformation that allowed direct coordination to form a six coordinate Fe complex as would be expected [36]. In addition, the heme conformation in the X-ray structure showed significant distortion from planarity and this was updated using a confirmation re-optimized in the gas phase at the Becke's three-parameter plus Lee–Yang–Parr (B3LYP) functional [49,50] with 6-31G* (with model SCH_3 and H_2O ligand). Molecular dynamics simulations were performed using the default CHARMM settings in Discovery Studio (DS) 2.5 program [51]. In addition, cofactors, ions, and water molecules beyond 15 Å of the active site were deleted. Missing atoms were added using CHARMm 22 force field [52] via the DS 2.5 program. The protonation states of ionizable residues were determined by the PROPKA program [53]. Histidine residues were specified as HID except for His_{345} and His_{404}, in which were protonated on the NE atom of imidazole and His_{164} with was protonated at both the NE and ND atoms. Ligand and heme charges were determined using HF/6-31G* ESP charges. The system was solvated in a cubic box of TIP3P water and counter ions were added to neutralize the system using DS.

The high resolution X-ray structure needed only minor preparation before QM/MM simulation to adjust to the updated heme conformation and the additional oxygen atom added to the substrate already present. The following procedure was applied; (1) hydrogen atoms alone were optimized in the first iteration, (2) all amino side chain atoms were optimized, except for the heme and the Fe—O distance, which were harmonically using default settings restrained (Fe—O distance set at 2.1 Å). Finally, (3) the backbone of the protein and the heme remained harmonically restrained and the protein was allowed to relax over a period of 1 ns of MD in DS 2.5 (heating 0.2 ps (0–300 K), equilibration, 0.5 ps and production 0.2 ps) with the same restraints described above in place. The RMSD between the X-ray and final MD structure backbones were computed at 0.70 Å confirming that only a subtle re-orientation of the protein occurred as a result of the active site modifications.

The 1 ns MD structure was used as an initial structure for QM cluster and QM/MM protein models. The active site of AOS is buried deep within the protein in which water molecules are not accessible. Thus, solvent water molecules were removed to reduce the computational requirement. A single water molecule placed within the active site pocket was retained to investigate the water assisted mechanism.

2.2. QM cluster and QM/MM protein calculations

Two different reaction mechanisms of AOS have been investigated by means of both a QM active site cluster model (B3LYP) and a QM/MM protein model (B3LYP:AMBER) where the active site is treated QM and the surrounding residues are treated using an MM force field. The QM cluster model consists of Fe-heme, the side chains of Cys_{471}, Asn_{321}, Phe_{137}, terminated at the Cα, and a truncated substrate (S3). Both the hydrogen and heavy atom across the

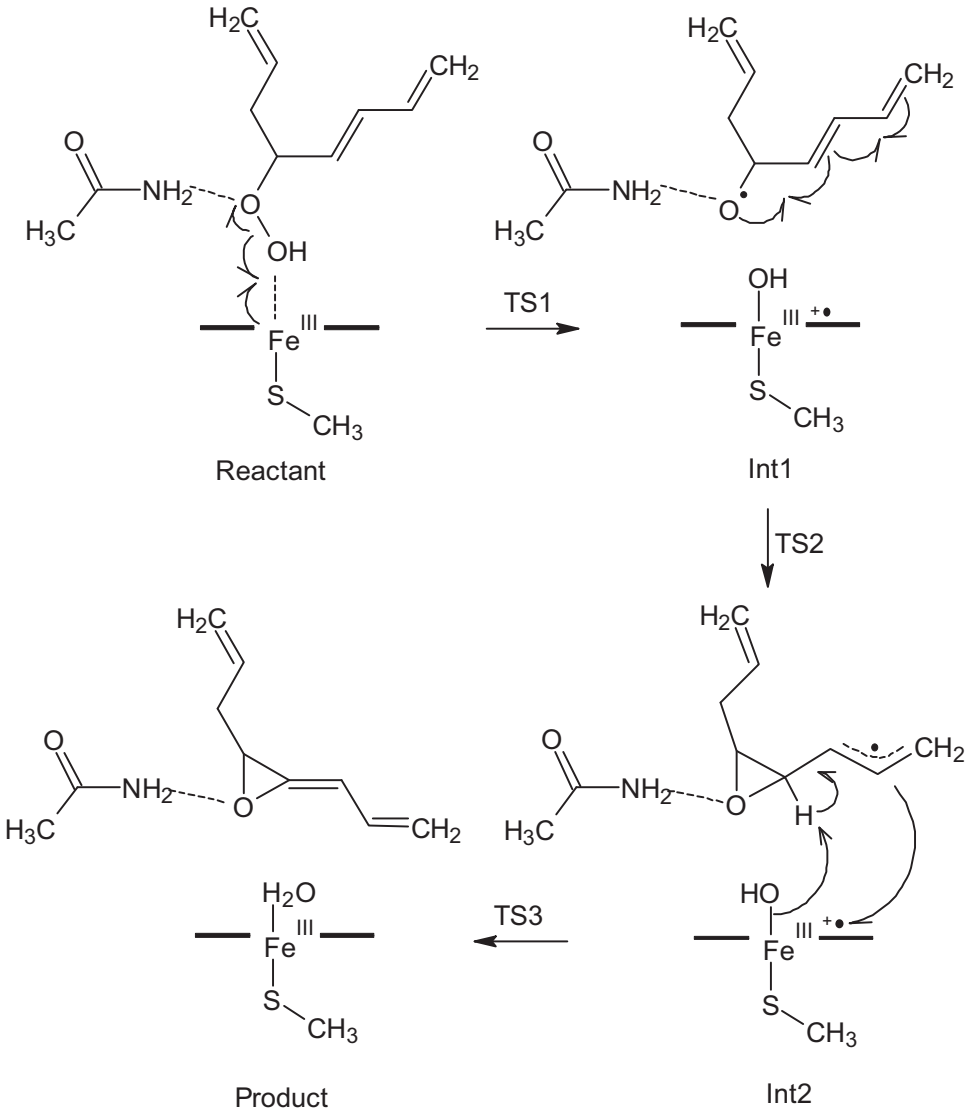

Scheme 1. A proposed reaction mechanism on plant AOS via the standard mechanism.

terminated side chain were frozen to limit the conformational flexibility of the residues. Hydrogen link atoms have been used as a QM/MM boundary (Fig. 1). As a result of the interactions with the heme and Phe_{137}, this restricts the active site to a conformation very similar to the full QM/MM model (S6). The QM/MM protein model consists of Fe—heme, the side chains of Cys_{471}, Asn_{321}, terminated at the Cα, and a truncated substrate as a QM region and the rest is treated as a MM region, because of more computational demanding. In contrast to QM cluster model, Phe_{137} residue is treated MM. All QM/MM protein optimization calculations were performed using the ONIOM methodology [54,55] with the electronic embedding (ONIOM-EE) scheme. Atoms within a distance of 15 Å from the Fe atom in the active site are flexible. Only doublet open-shell species ($S = 1/2$; S refers to total spin angular momentum) was considered, because previous QM cluster studies for thromboxane and prostacyclin biosynthesis studies show that the quartet and sextet states were found to be higher in energy for O—O bond dissociation [37,38,45].

The QM region used in the QM/MM model consists of 73 atoms with 663 basis functions (or 76 atoms with 671 basis functions with additional water). The total charge of the QM region is neutral. The gasphase QM model consists of 88 atoms (Phe137 included QM) with 775 basis functions (or 91 atoms with 793 basis functions with additional water). The total charge of the model is also neutral. All QM and QM/MM calculations were performed in the Gaussian 09 program [56]. Structure optimizations were performed using the B3LYP functional with TZVP (Fe) and 6-31G* basis sets (remaining atoms). The B3LYP approach has revealed in reproducing many experimental properties and has been considered to be a preferable approach for enzyme P450 system [3,57]. All structures were fully characterized using normal coordinate analysis and the free energy corrections based on B3LYP/TZVP-6-31G*. Single point calculations for the gas phase models were obtained at both B3LYP and B3LYP* functionals [58] with the following basis sets TZVP (Fe) and 6-311+G** (remaining atoms). The B3LYP method only was used to obtain QM/MM (ONIOM-EE) single point energies.

3. Results

The standard and alternative reaction mechanisms have been investigated shown in Schemes 1 and 2, respectively. Scheme 1 can be considered as analog to that proposed by Cho et al., differing only in that for the 1st step the peroxide heme is bound to the Fe-heme. The 2nd process assesses the effect of water molecule on the process and whether it can play a stabilizing role in the proton shuttle process as found in other P450 studies [39,40]. The optimized

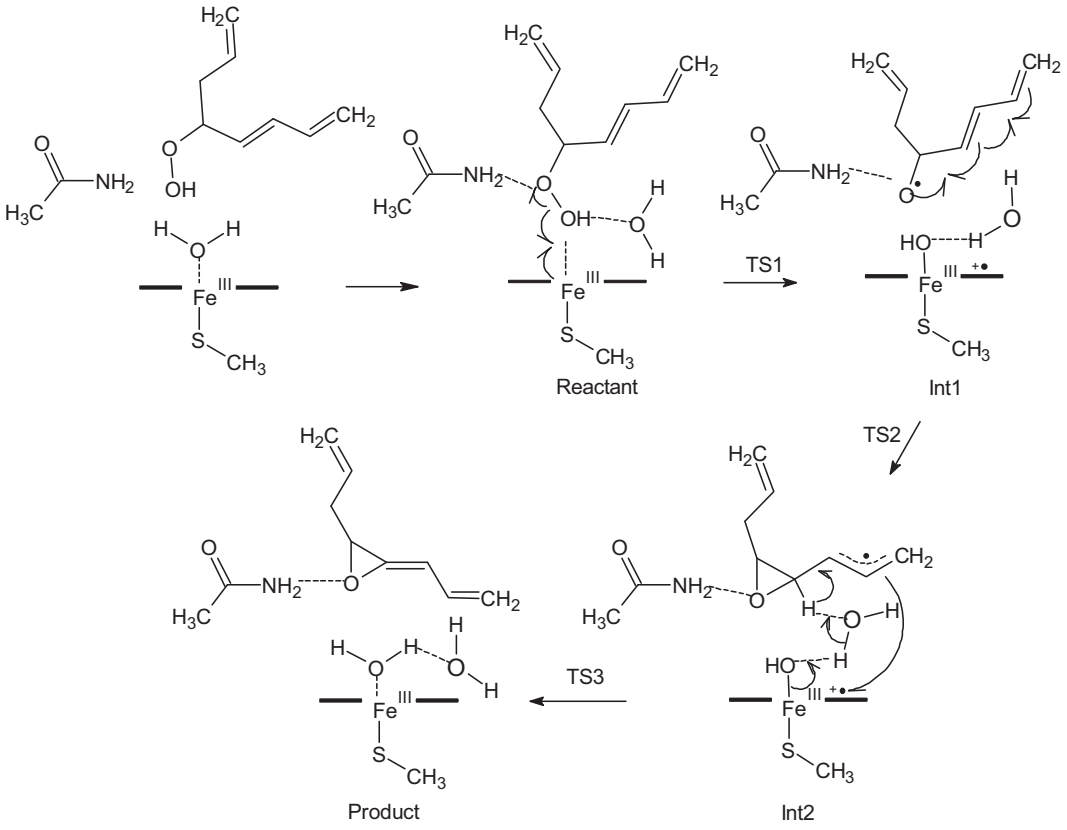

Scheme 2. A proposed reaction mechanism on plant AOS via an alternative mechanism.

structures and Mulliken spin density obtained on the potential energy surface are shown in Figs. 2 and 3. All energies are reported relative to the corresponding reactant in kcal/mol. B3LYP* and B3LYP single points energies were found to be comparable to both the optimized B3LYP and free energy corrected values. We therefore discuss only the B3LYP/6-31G* or ONIOM(B3LYP/6-31G*:AMBER) free energies unless otherwise stated. All computed energies can be found in S10 in the electronic supplementary material.

Both reaction mechanisms (standard vs water mediated proton shuttle) proceed with 4 steps; (1) the fatty acid hydroperoxide (reactant) bound to Fe^{III}-porphyrin, (2) then homolytic O—O bond cleavage occurs as intermediate 1 (Int1) via Fe^{III} and Fe^{IV} pathways, (3) epoxide formation as intermediate 2 (Int2) and (4) leading to allene oxide formation as a product. The results obtained from a standard mechanism on QM cluster model will be firstly discussed followed by QM/MM protein model and an alternative mechanism.

3.1. Standard mechanism of AOS: QM cluster and QM/MM protein models

The standard mechanism shown in Scheme 1 starts with iron hexa-coordinate heme with the substrate bounds to Fe^{III} for 2.42 Å on QM cluster model (Fig. 2). This differs from the work of Cho et al. [37] who investigated a reaction starting with a heme unbound conformation. Our study begins with the bound (doublet) which is found to be ~2 kcal/mol lower in energy than the corresponding unbound sextet state (See supplementary information Fig. S11).

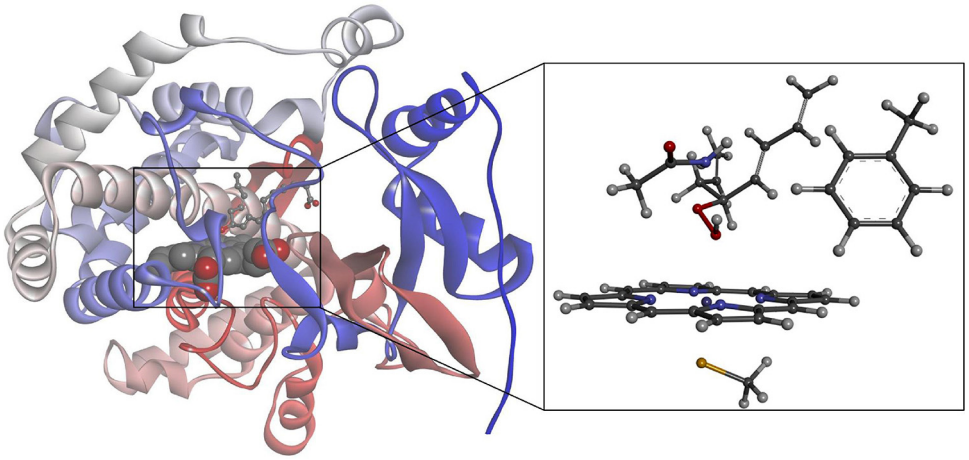

Fig. 1. The 3D structure of AOS (cytochrome P450 74A, CYP74A) complexed with 13(*S*)-HPOT at 1.60 Å resolution (left; [8]) and QM model (right).

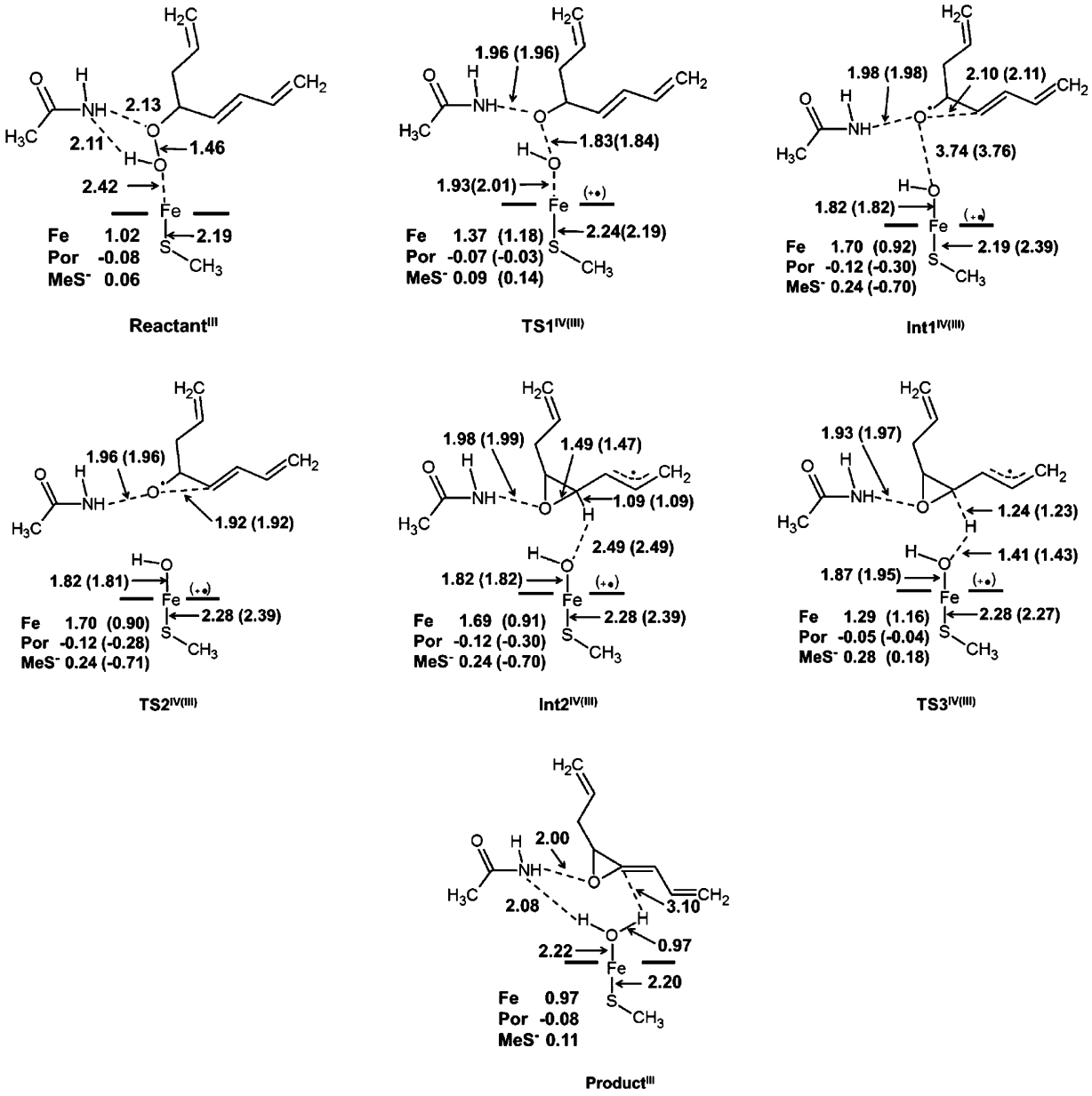

Fig. 2. Optimized structures of QM cluster model on standard mechanism. The selected atomic distances are shown in angstroms (Å) and in parentheses for Fe^{III}, and Mulliken spin densities of Fe, Porphyrin (Por) and Cysteine residue (MeS^-) are shown.

Thus this initial configuration is consistent with the work of Bushnell et al. who studied coral AOS [42]. Nevertheless, the active site configuration in coral AOS differs from plant AOS, having a histidine residue (His_{67}) adjacent to the substrate, which plays a role in a proton transfer from the peroxide moiety. In plant AOS, while the adjacent Asn_{321} residue can interact with the ROOH proton, the amide group is incapable of accepting a proton. Understandably it is found that the intermediates found along the reaction mechanisms between coral and plant AOS are different. Therefore, the structural and energetic properties between these two enzymes are not discussed in detail.

The homolytic O—O bond cleavage leads to an oxygen radical intermediate (Int1) which is very similar in configuration to that found by Cho et al. [37]. This is notable given the rather different starting structures (Fe bound vs unbound respectively). In this study the Fe—OH bond is formed with 1.82 Å and the O—O bond tears apart from 1.46 Å to 3.74 Å. Int1 is shifted further away from Fe-heme center and the hydrogen bond between oxygen radical and Asn_{321} (O···HN) becomes stronger (1.98 Å). The activation energy requires for the homolytic O—O bond cleavage is 13.0 kcal/mol via the $TS1^{III}$, whereas the $TS1^{IV}$ requires 12.4 kcal/mol (Fig. 4). It was found in previous investigations of different AOS types that O—O bond cleavage resulted in a transition state of 12.9 kcal/mol (Fe^{III}) for plant AOS [37] and is 23.8 kcal/mol (Fe^{IV}) for coral AOS [42].

Next, an epoxide is then formed with no barrier for $TS2^{III}$, whereas $TS2^{IV}$ requires 0.9 kcal/mol. The C—O bond distance changes from $Int1^{IV(III)}$, $TS2^{IV(III)}$ and $Int2^{IV(III)}$ are 2.10 (2.11) Å, 1.92 (1.92) Å and 1.49 (1.47) Å, respectively. The Fe—OH bond is maintained to ~1.82 Å both in Fe^{III} and Fe^{IV} pathways. The epoxide formation drops down the energy of $Int2^{III}$ and $Int2^{IV}$ to −6.3 and −10.6 kcal/mol, respectively. The final step is the PCET mechanism to obtain allene oxide formation. The proton is shuttled (H···OH) by the distance 2.49 Å of Int2 to product with 0.97 Å via $TS3^{IV(III)}$ with 1.41 (1.43) Å of H···OH distance. The spin density of the transferring hydrogen of −0.04

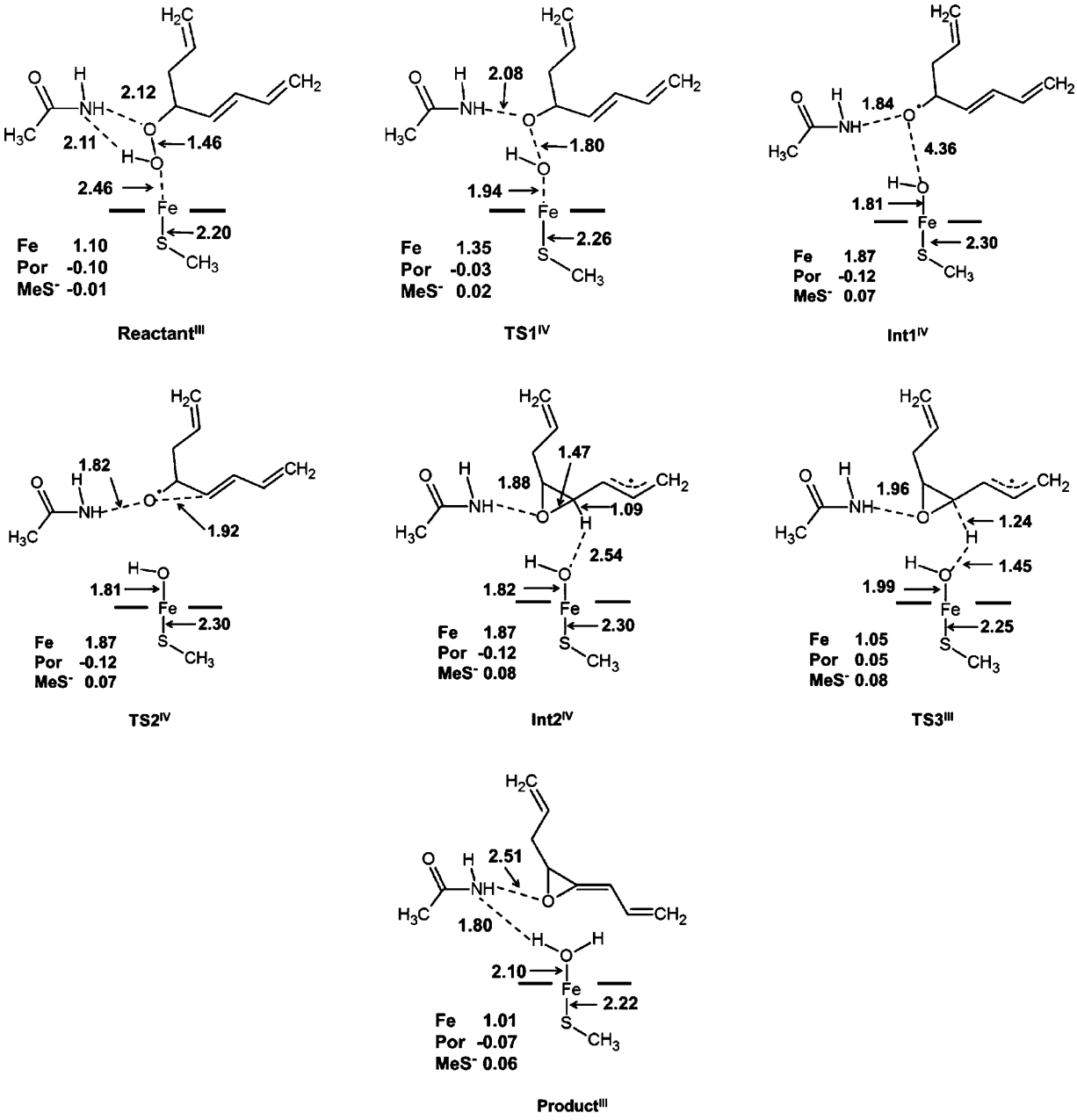

Fig. 3. Optimized structures of QM/MM protein model. The selected atomic distances are shown in angstroms (Å) and Mulliken spin densities of Fe, Porphyrin (Por) and Cysteine residue (MeS^-) are shown.

for $TS3^{IV}$ is very low as expected in PCET mechanism rather than hydrogen atom transfer (HAT) mechanism. The activation energies of this step are 11.5 and 16.9 kcal/mol via Fe^{III} and Fe^{IV} pathway, respectively. The $TS3^{IV}$ requires higher activation energy than $TS3^{III}$ because $Int2^{IV}$ is lower in energy than $Int2^{III}$ (−10.6 vs −6.3 kcal/mol). Allene oxide product is formed with −34.6 kcal/mol. The hydrogen bond NH···O distance (between Asn_{321} and epoxide moiety of the substrate) is maintained about 2.0 Å along the reaction profile. The equivalent to $TS3^{III}$ from the previously reported plant AOS study was found to be considerably lower at 4.9 kcal/mol [37]. Microsolvation calculations using the QM cluster model have been tested. The results as applied to the standard mechanism show that the cysteine charges observed along the reaction coordinate are comparable with the gas phase calculations (S12).

The higher activation energy in our study compared to Cho et al. [37] is in part due to the higher stability of Int Fe^{III}, but also due to a higher absolute barrier. This appears to be due to the more dissociated reactant starting configuration (i.e. weaker Fe bindings in the reactant) which allows for greater flexibility in the final step, leading to the lower energy proton transfer step. The energies do show considerable dependence on the method and basis set suggesting the barrier is very method sensitive (dissociative structure) and higher level single point energies may not be appropriate on low level geometries. For the study of Cho et al. the energy of $TS3^{III}$ decreases with increasing level of theory (6.2, 4.9 and 3.0 kcal/mol) calculated by B3LYP/LACVP (ΔH), B3LYP/LACV3P*+ (ΔH) and B3LYP/LACV3P (ΔG), respectively. In this study, $TS3^{III}$ was found to be 11.9, 14.6, and 11.5 kcal/mol obtained from B3LYP/6-31G* (ΔH), B3LYP/6-311+G** (ΔH) and B3LYP/6-31G* (ΔG) gas-phase calculations, respectively. The corresponding QM/MM values were 16.5, 13.4, and 22.4 kcal/mol obtained from B3LYP/6-31G* (ΔH), B3LYP/6-311+G** (ΔH) and B3LYP/6-31G* (ΔG), respectively.

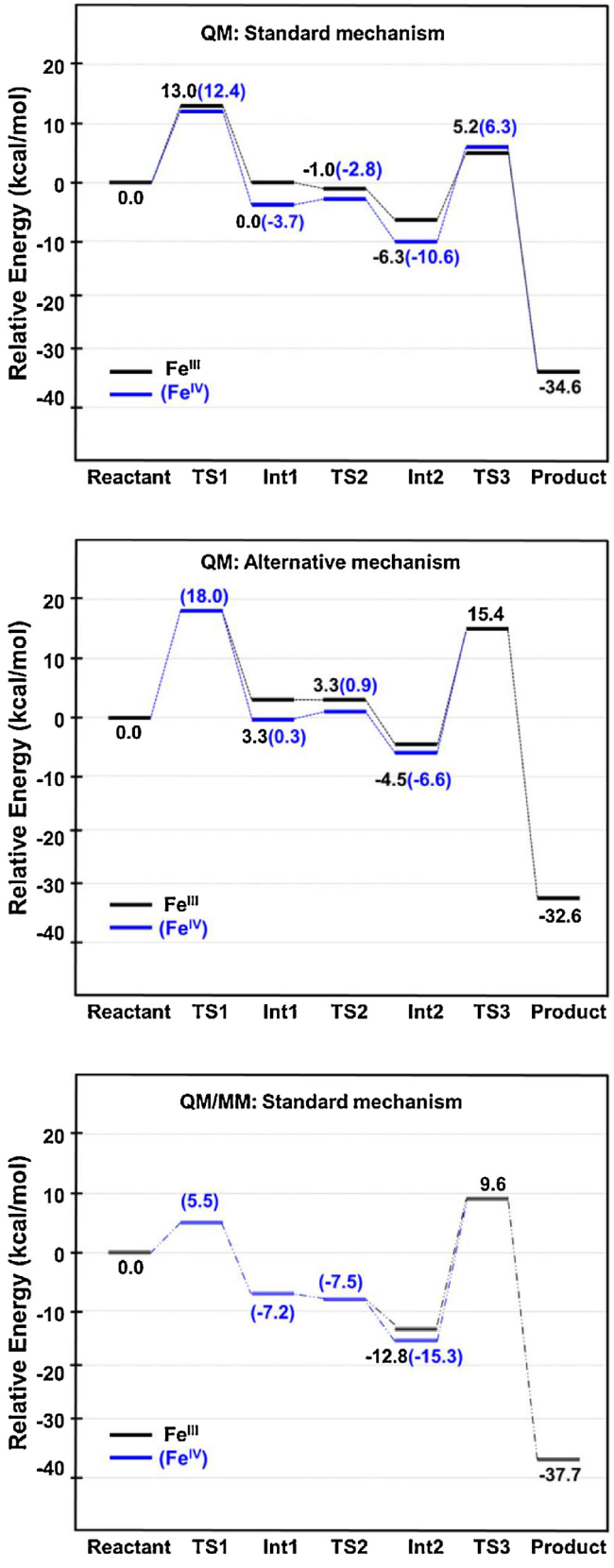

Fig. 4. Reaction profile of plant AOS mechanism comparing between Fe^{III} and Fe^{IV} pathways of standard mechanism on QM cluster model (top) and QM/MM protein model (middle) and alternative mechanism on QM cluster model (bottom).

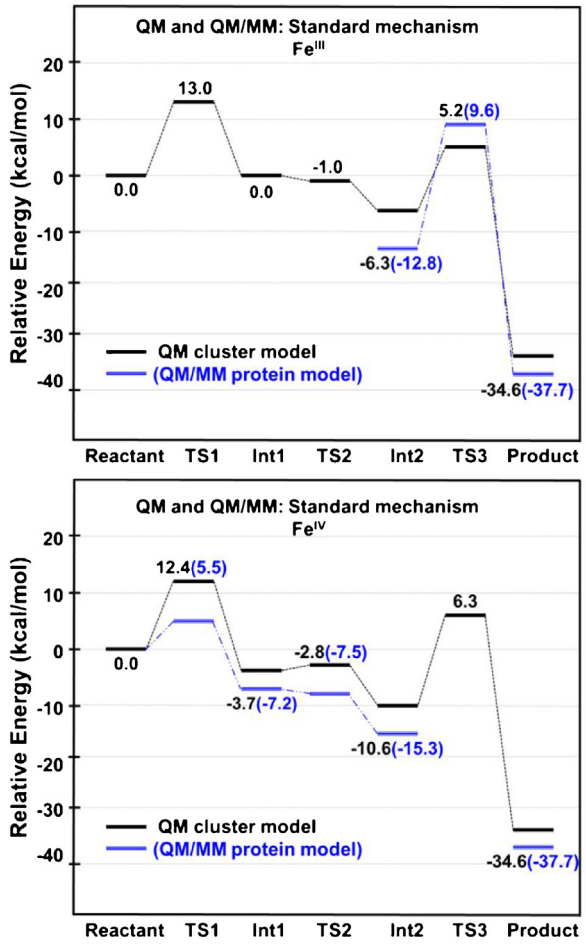

Fig. 5. Reaction profile of plant AOS mechanism of the standard mechanism comparing between QM cluster model and QM/MM protein model on Fe^{III} pathway (top) and Fe^{IV} pathway (bottom).

Analysis of the results show that the Fe^{III} based pathway is very similar to that of the Fe^{IV} pathway (Fig. 5). However, the rate determining step for Fe^{III} pathway is the O—O bond cleavage requiring 13.0 kcal/mol, whereas it is found to be the final PCET (16.9 kcal/mol) for Fe^{IV}. The results appear to show that Fe^{IV} pathway is energetically less preferable because of the stability of local minima results in a slightly higher barrier for the final step Fig. 6.

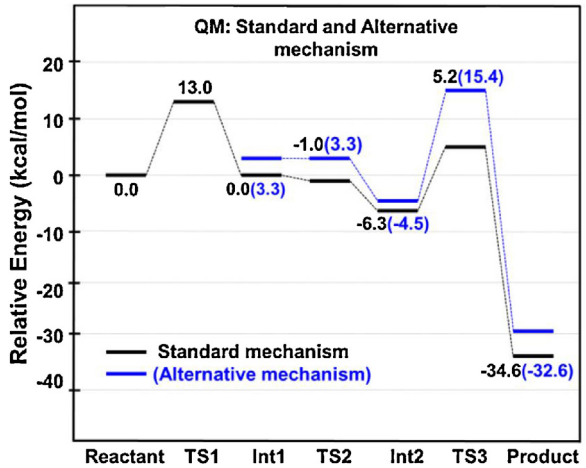

Fig. 6. Reaction profile of plant AOS mechanism on Fe^{III} pathway comparing between standard mechanism and alternative mechanism on QM cluster model.

3.2. QM/MM study on the standard mechanism

The structures obtained from the QM/MM model are found to closely resemble those of the QM calculations, even though the latter was performed in the gas phase. In the QM/MM protein model it is found that the substrate is bound to the heme Fe at 2.46 Å, which compares to 2.42 in the QM cluster model. Moreover, the key distances involved in the catalytic process found in both models are found to be similarly ideal (Figs. 2 and 3).

The QM/MM activation energy of the homolytic O—O bond cleavage is 5.5 kcal/mol (Fig. 4), which is lower than that observed for QM cluster model (12.4 kcal/mol). Electrostatic interaction between QM region and protein point charges of MM region embedded in QM calculations leads to the larger difference as confirmed by a gas-phase single point energy calculation on the QM/MM optimized conformation (see S13). The structural properties of $TS1^{IV}$ QM cluster model and QM/MM protein model are similar. The O···O distance of $Int1^{IV}$ found in QM/MM protein model is longer (4.36 Å) than that found in QM cluster model (3.76 Å), and the hydrogen bond between the oxygen radical and Asn_{321} becomes stronger. Notably, it is found that the key distances involved in the reaction mechanism obtained by QM cluster model and QM/MM protein model are similar (S3 and Fig. 2). $Int1^{IV}$ is lower in energy (−7.2 kcal/mol) compared with QM cluster model (−3.7 kcal/mol) and the epoxide formation occurs with no activation energy ($TS2^{IV}$ is −7.5 kcal/mol). The $Int2^{IV}$ is also found to be lower in energy (−15.3 kcal/mol) compared to $Int2^{III}$ (−12.8 kcal/mol) as also found in QM cluster model. In this study, we are not able to obtain $TS1^{III}$, $Int1^{III}$ and $TS2^{III}$. However, QM cluster model already shows that the optimized structures of Fe^{III} and Fe^{IV} species are similar. Geometry optimization of $TS1^{III}$ led to $TS1^{IV}$ (*vide infra*). Lastly, the $Int2^{III}$ requires 22.4 kcal/mol leading to the product through $TS3^{III}$ (−37.7 kcal/mol). The results demonstrate that the rate determining step in the QM/MM protein model is the PCET step. This is because the protein stabilizes TS1 more than TS3 (S13).

Efforts to obtain Fe^{III} intermediates and transitions states proved unsuccessful. It was found that during the optimization of Fe^{III} structures (TS1, Int1 and TS2) the final converged conformation converted back to Fe^{IV} configuration. For TS3, the opposite was observed. The results of our QM/MM protein model shows that Fe^{III} route is preferably, in good agreement with Cho et al. [37], however the barrier is somewhat higher (22.4 kcal/mol) than for both QM (11.5 kcal/mol) and Cho et al. (3 kcal/mol) [37]. This difference is primarily down to the much greater stability of Int2 compared to Cho et al. [37]. Furthermore, the single point energy of QM/MM TS3 is just 13.4 kcal/mol, which is closer to the expected experimental value [37].

It is noted that we start from a considerably different starting conformation than Cho et al. [37], in our case with the substrate directly coordinated to the Fe, which does lead to subtle differences in the reaction profile. Our QM and QM/MM results show that local minima reaction species are more stable, which was not the case for the former study. Similarly, our QM calculations also reveal that Fe^{IV} local minima species are more stable than Fe^{III}, thereby leading to higher activation energy in TS3. From our QM and QM/MM predictions the rate determining step could indeed involve either Fe spin state, and plausibly be either TS1 or TS3 given their comparable energetic overall.

3.3. Water assisted proton shuttle mechanism

The optimized structures of the alternate, a water assisted proton shuttle mechanism, are shown in the electronic supplementary material (S8). The overall reaction profile of this alternative mechanism is broadly equivalent to the standard mechanism. The substrate is bound to Fe-heme 2.42 Å as found in the standard mechanism. An additional water molecule is hydrogen bonded to the peroxide moiety at 1.74 Å. The reaction proceeds to Int1 by of the breaking of the O—O bond. The activation energy required for the O—O bond cleavage is 18.0 kcal/mol. The substrate experiences a shift away from the Fe-heme center and the O···O bond distance elongates to 4.46 and 4.36 Å for $Int1^{IV}$ and $Int1^{III}$, respectively. It is noted that the O···O bond distance in alternative mechanism is longer than that found in the standard mechanism (3.74 and 3.76 Å). The hydroxyl group of $Int1^{IV}$ is bound to Fe-heme for 1.89 Å. It is found that the additional water molecule maintains a strong hydrogen bond (1.8 Å on average) with the hydroxyl group. Correspondingly, the additional water molecule also maintains its hydrogen bond H···NH to Asn_{321} about 2.1 Å. The hydrogen bond between Asn_{321} and substrate (NH···O) distance is about 2.0 Å similarly to those found in the standard mechanism (S7). Although it is found that the substrate is shifted further away from the Fe-heme center because of an additional water molecule, but it is found that the key distances are quite similar to those found in standard mechanism. The additional water molecule raises the barrier, thus not facilitating the proton transfer. The TS3 is 15.4 kcal/mol, showing that the additional water molecule in-fact destabilizes TS3 unlike reports elsewhere [59,60]. This result agrees with the study of de Visser et al. in which hydrogen bonding interactions reduce the catalytic activity in Fe(IV)-oxo biomimetic complexes [61]. In addition, additional water molecules were predicted to increase the activation barrier of the PCET between close Tyr radical and Cys residues in the different peptide chains in protein molecules by model DFT calculations [41].

4. Conclusions

In this study we make use of a recently reported high resolution X-ray structure to assess the catalytic processes occurring within AOS at the atomic level. Two different reaction mechanisms have been investigated by QM and QM/MM (ONIOM) calculations with B3LYP density functional. Both the QM and QM/MM results showed considerable concordance, giving us confidence that the cluster models had a good degree of realism. This confirms that the large active site cluster model is a reasonable approximation for the whole protein. Our calculations suggest that the Fe^{IV} local minima are comparable in energy to Fe^{III}, thereby leading to higher activation energy at the final barrier (TS3). The results also show that the transition state of O—O bond cleavage (TS1) and proton couple electron transfer (TS3) are very similar in term of energy. QM calculations reveal that the reaction can undergo for both Fe^{III} and Fe^{IV} pathway as the energy profile are equivalent. From our QM and QM/MM predictions the rate determining step could indeed involve either Fe spin state, and plausibly be either TS1 or TS3, given their comparable energetic overall.

The results for the standard mechanism are also similar to those found by Cho and co-workers [37], even though we used a more optimal starting heme on figuration with a 6-coordinate heme, substrate bound conformation. Subtle differences in results are not unexpected given that both are based on different models, relying on single conformations. The former is based on known X-ray structure with a non-substrate, and ours based on a modified X-ray structure containing the substrate which was prepared to ideal Fe bound substrate starting configuration. While the rate determining step in our study is found later on the reaction coordinate (TS3 vs TS1 respectively), the general conclusions are not incompatible given that Cho et al. also noted that both spins states were possible.

The key issue in this study was whether the PCET reaction mechanism in pAOS could be facilitated by an additional bound water molecule as found for related proteins. We have also explored the

effect of additional water molecule on the reaction mechanism using our QM cluster model, however, we find the process to be energetically less favorable compared to the non-water mediated proton transfer process. We find that the proton couple electron transfer (PCET) via an additional water molecule requires considerably higher activation energy (19.9 vs 11.5 kcal/mol) than direct mechanism. This suggests that the earlier findings, that a PCET mechanism can lead to a lower mechanism, may not be general to other closely related family members.

Acknowledgments

This work was supported by the Thailand Research Fund (TRF) through a Senior Research Scholar (RTA5380010). T.S. is grateful to the Royal Golden Jubilee Program for a scholarship (3.C.KU/53/B.1) and to Faculty of Science, Kasetsart University for Budget for Overseas Academic Conferences (BOAC). This work was supported by Grant-in-Aid for Scientific Research on Innovative Areas "Molecular Activation Directed toward Straightforward Synthesis", No. 23105507 from JSPS KAKENHI, Japan, to S.M. We also acknowledge the Laboratory for Computational and Applied Chemistry (LCAC), Kasetsart University Research and Development Institute (KURDI) the Commission on Higher Education, Ministry of Education [through the "National Research University Project of Thailand (NRU)" and "National Center of Excellence for Petroleum, Petrochemical Technology and Advance Materials (NCEPPAM)"], and Research Center for Computational Science (RCCS), the National Institutes of Natural Sciences, Japan are also acknowledged for generous support and research facilities.

Appendix A. Supplementary data

Supplementary data associated with this article can be found, in the online version, at http://dx.doi.org/10.1016/j.jmgm.2014.05.012.

References

[1] S.S.T. Lee, J.T.M. Buters, T. Pineau, P. Fernandez-Salguero, F.J. Gonzalez, Role of CYP2E1 in the hepatotoxicity of acetaminophen, J. Biol. Chem. 271 (20) (1996) 12063–12067.
[2] O. Beck, N. Stephanson, R.G. Morris, B.C. Sallustio, P. Hjemdahl, Determination of perhexiline and hydroxyperhexiline in plasma by liquid chromatography–mass spectrometry, J. Chromatogr. B: Analyt. Technol. Biomed. Life Sci. 805 (1) (2004) 87–91.
[3] P.R. Ortiz de Montellano, Cytochrome P450, in: Structure, Mechanism, and Biochemistry, Kluwer Academic/Plenum Publishers, New York, 2005, pp. 689.
[4] A. Sigel, H. Sigel, R.K.O. Sigel, The Ubiquitous Role of Cytochrome P450 Proteins in Metal Ions in Life Sciences, 2007.
[5] R. Fasan, Tuning P450 enzymes as oxidation catalysts, ACS Catal. 2 (4) (2012) 647–666.
[6] L.I. Gilbert, Halloween genes encode P450 enzymes that mediate steroid hormone biosynthesis in *Drosophila melanogaster*, Mol. Cell. Endocrinol. 215 (1–2) (2004) 1–10.
[7] D.R. Harder, A.R. Lange, D. Gebremedhin, E.K. Birks, R.J. Roman, Cytochrome P450 metabolites of arachidonic acid as intracellular signaling molecules in vascular tissue, J. Vasc. Res. 34 (3) (1997) 237–243.
[8] D.M. Stocco, StAR protien and the regulation of steroid hormone biosynthesis, Annu. Rev. Physiol. 63 (1) (2001) 193–213.
[9] X. Ding, L.S. Kaminsky, Human extrahepatic cytochromes P450: function in xenobiotic metabolism and tissue-selective chemical toxicity in the respiratory and gastrointestinal tracts, Annu. Rev. Pharmacol. Toxicol. 43 (1) (2003) 149–173.
[10] F.J. Gonzalez, A.-M. Yu, Cytochrome P450 and xenobiotic receptor humanized mice, Annu. Rev. Pharmacol. Toxicol. 46 (1) (2006) 41–64.
[11] M.C.U. Gustafsson, O. Roitel, K.R. Marshall, M.A. Noble, S.K. Chapman, A. Pessegueiro, A.J. Fulco, M.R. Cheesman, C. von Wachenfeldt, A.W. Munro, Expression, purification, and characterization of *Bacillus subtilis* cytochromes P450 CYP102A2 and CYP102A3: flavocytochrome homologues of P450 BM3 from *Bacillus megaterium*, Biochemistry 43 (18) (2004) 5474–5487.
[12] C. Helvig, N. Tijet, R. Feyereisen, F.A. Walker, L.L. Restifo, *Drosophila melanogaster* CYP6A8, an insect P450 that catalyzes lauric acid (ω-1)-hydroxylation, Biochem. Biophys. Res. Commun. 325 (4) (2004) 1495–1502.
[13] D.R. Davydov, E.V. Sineva, N.Y. Davydova, D.H. Bartlett, J.R. Halpert, CYP261 enzymes from deep sea bacteria: a clue to conformational heterogeneity in cytochromes P450, Biotechnol. Appl. Biochem. 60 (1) (2013) 30–40.
[14] K.S. Rabe, M. Erkelenz, K. Kiko, C.M. Niemeyer, Peroxidase activity of bacterial cytochrome P450 enzymes: modulation by fatty acids and organic solvents, Biotechnol. J. 5 (8) (2010) 891–899.
[15] K.-L. Ku, P.-S. Chang, Y.-C. Cheng, C.-Y. Lien, Production of stilbenoids from the callus of *Arachis hypogaea*: a novel source of the anticancer compound piceatannol, J. Agric. Food Chem. 53 (10) (2005) 3877–3881.
[16] M. Morant, S. Bak, B.L. Møller, D. Werck-Reichhart, Plant cytochromes P450: tools for pharmacology, plant protection and phytoremediation, Curr. Opin. Biotechnol. 14 (2) (2003) 151–162.
[17] M. Morant, K. Jørgensen, H. Schaller, F. Pinot, B.L. Møller, D. Werck-Reichhart, S. Bak, CYP703 is an ancient cytochrome P450 in land plants catalyzing in-chain hydroxylation of lauric acid to provide building blocks for sporopollenin synthesis in pollen, Plant Cell. 19 (5) (2007) 1473–1487.
[18] K. Matsui, M. Shibutani, T. Hase, T. Kajiwara, Bell pepper fruit fatty acid hydroperoxide lyase is a cytochrome P450 (CYP74B), FEBS Lett. 394 (1) (1996) 21–24.
[19] O. Boutaud, A.R. Brash, Purification and catalytic activities of the two domains of the allene oxide synthase-lipoxygenase fusion protein of the coral *Plexaura homomalla*, J. Biol. Chem. 274 (47) (1999) 33764–33770.
[20] E. Psylinakis, E.M. Davoras, N. Ioannidis, M. Trikeriotis, V. Petrouleas, D.F. Ghanotakis, Isolation and spectroscopic characterization of a recombinant bell pepper hydroperoxide lyase, Biochim. Biophys. Acta 1533 (2) (2001) 119–127.
[21] M. Stumpe, J. Bode, C. Göbel, T. Wichard, A. Schaaf, W. Frank, M. Frank, R. Reski, G. Pohnert, I. Feussner, Biosynthesis of C9-aldehydes in the moss *Physcomitrella patens*, Biochim. Biophys. Acta 1761 (3) (2006) 301–312.
[22] M. Hamberg, H.W. Gardner, Oxylipin pathway to jasmonates: biochemistry and biological significance, Biochim. Biophys. Acta 1165 (1) (1992) 1–18.
[23] D.-S. Lee, P. Nioche, M. Hamberg, C.S. Raman, Structural insights into the evolutionary paths of oxylipin biosynthetic enzymes, Nature 455 (7211) (2008) 363–368.
[24] M.J. Mueller, Radically novel prostaglandins in animals and plants: the isoprostanes, Chem. Biol. 5 (12) (1998) R323–R333.
[25] D.B. Neau, N.C. Gilbert, S.G. Bartlett, W. Boeglin, A.R. Brash, M.E. Newcomer, The 1.85 Å structure of an 8R-lipoxygenase suggests a general model for lipoxygenase product specificity, Biochemistry 48 (33) (2009) 7906–7915.
[26] M.L. Oldham, A.R. Brash, M.E. Newcomer, The structure of coral allene oxide synthase reveals a catalase adapted for metabolism of a fatty acid hydroperoxide, Proc. Natl. Acad. Sci. U. S. A. 102 (2) (2005) 297–302.
[27] L. Li, Z. Chang, Z. Pan, Z.-Q. Fu, X. Wang, Modes of heme binding and substrate access for cytochrome P450 CYP74A revealed by crystal structures of allene oxide synthase, Proc. Natl. Acad. Sci. U. S. A. 105 (37) (2008) 13883–13888.
[28] M. Altarsha, D. Wang, T. Benighaus, D. Kumar, W. Thiel, QM/MM study of the second proton transfer in the catalytic cycle of the D251N mutant of cytochrome P450cam, J. Phys. Chem. B 113 (28) (2009) 9577–9588.
[29] T. Rungrotemongkol, A.J. Mulholland, S. Hannongbua, QM/MM simulations indicate that Asp185 is the likely catalytic base in the enzymatic reaction of HIV-1 reverse transcriptase, MedChemComm 5 (2014) 593–596.
[30] N.M. Thellamurege, H. Hirao, Effect of protein environment within cytochrome P450cam evaluated using a polarizable-embedding QM/MM method, J. Phys. Chem. B 118 (8) (2014) 2084–2092.
[31] H. Hirao, P. Chuanprasit, Y.Y. Cheong, X. Wang, How is a metabolic intermediate formed in the mechanism-based inactivation of cytochrome P450 by using 1,1-dimethylhydrazine: hydrogen abstraction or nitrogen oxidation? Chemistry 19 (23) (2013) 7361–7369.
[32] D. Li, X. Huang, K. Han, C.-G. Zhan, Catalytic mechanism of cytochrome P450 for 5′-hydroxylation of nicotine: fundamental reaction pathways and stereoselectivity, J. Am. Chem. Soc. 133 (19) (2011) 7416–7427.
[33] D. Li, Y. Wang, K. Han, Recent density functional theory model calculations of drug metabolism by cytochrome P450, Coord. Chem. Rev. 256 (11–12) (2012) 1137–1150.
[34] R. Lonsdale, K.T. Houghton, J. Żurek, C.M. Bathelt, N. Foloppe, M.J. de Groot, J.N. Harvey, A.J. Mulholland, Quantum mechanics/molecular mechanics modeling of regioselectivity of drug metabolism in cytochrome P450 2C9, J. Am. Chem. Soc. 135 (21) (2013) 8001–8015.
[35] B. Meunier, S.P. de Visser, S. Shaik, Mechanism of oxidation reactions catalyzed by cytochrome P450 enzymes, Chem. Rev. 104 (9) (2004) 3947–3980.
[36] S. Shaik, S. Cohen, Y. Wang, H. Chen, D. Kumar, W. Thiel, P450 enzymes: their structure, reactivity, and selectivity—modeled by QM/MM calculations, Chem. Rev. 110 (2) (2009) 949–1017.
[37] K.B. Cho, W. Lai, M. Hamberg, C.S. Raman, S. Shaik, The reaction mechanism of allene oxide synthase: interplay of theoretical QM/MM calculations and experimental investigations, Arch. Biochem. Biophys. 507 (1) (2011) 14–25.
[38] T.K. Yanai, S. Mori, Density functional studies on isomerization of prostaglandin H_2 to prostacyclin catalyzed by cytochrome P450, *Chem. Eur. J.* 15 (17) (2009) 4464–4473.
[39] L. Tian, R.A. Friesner, QM/MM simulation on P450 BM3 enzyme catalysis mechanism, J. Chem. Theory Comput. 5 (5) (2009) 1421–1431.
[40] B. Zhao, F.P. Guengerich, M. Voehler, M.R. Waterman, Role of active site water molecules and substrate hydroxyl groups in oxygen activation by cytochrome P450 158A2: a new mechanism of proton transfer, J. Biol. Chem. 280 (51) (2005) 42188–42197.

[41] X. Chen, G. Ma, W. Sun, H. Dai, D. Xiao, Y. Zhang, X. Qin, Y. Liu, Y. Bu, Water promoting electron hole transport between tyrosine and cysteine in proteins via a special mechanism: double proton coupled electron transfer, J. Am. Chem. Soc. 136 (12) (2014) 4515–4524.
[42] E.A.C. Bushnell, R. Gherib, J.W. Gauld, Insights into the catalytic mechanism of coral allene oxide synthase: a dispersion corrected density functional theory study, J. Phys. Chem. B 117 (22) (2013) 6701–6710.
[43] P.E.M. Siegbahn, F. Himo, The quantum chemical cluster approach for modeling enzyme reactions, J. Biol. Inorg. Chem. 1 (3) (2011) 323–336.
[44] T. Tanabe, V. Ullrich, Prostacyclin and thromboxane synthases, J. Lipid Mediat. Cell Signal. 12 (2–3) (1995) 243–255.
[45] T.K. Yanai, S. Mori, Density functional studies on thromboxane biosynthesis: mechanism and role of the heme-thiolate system, Chem. Asian J. 3 (11) (2008) 1900–1911.
[46] T.K. Yanai, S. Mori, Mechanistic insights into prostanoid transformations catalyzed by cytochrome P450. Prostacyclin and thromboxane biosyntheses Adv. Med. Biol., 15, Nova Science Publishers, Inc., Hauppauge, NY, USA, 2011, pp. 231–253.
[47] S.P. de Visser, F. Ogliaro, P.K. Sharma, S. Shaik, What factors affect the regioselectivity of oxidation by cytochrome P450? A DFT study of allylic hydroxylation and double bond epoxidation in a model reaction, J. Am. Chem. Soc. 124 (39) (2002) 11809–11826.
[48] S. Shaik, S.P. de Visser, F. Ogliaro, H. Schwarz, D. Schröder, Two-state reactivity mechanisms of hydroxylation and epoxidation by cytochrome P-450 revealed by theory, Curr. Opin. Chem. Biol. 6 (5) (2002) 556–567.
[49] A.D. Becke, Density-functional thermochemistry III. The role of exact exchange, J. Chem. Phys. 98 (7) (1993) 5648–5652.
[50] C. Lee, W. Yang, R.G. Parr, Development of the Colle-Salvetti conelation energy formula into a functional of the electron density, Phys. Rev. B 37 (2) (1988) 785–789.
[51] Discovery Studio, Release 2.5.5, Accelrys Software Inc., San Diego, CA, USA, 2010.
[52] A.D. Mackerell, Empirical force fields for biological macromolecules: overview and issues, J. Comput. Chem. 25 (13) (2004) 1584–1604.
[53] J.H. Jensen, PROPKA, Copenhagen, Denmark, 2010.
[54] S. Dapprich, I. Komaromi, K.S. Byun, K. Morokuma, M.J. Frisch, A new ONIOM implementation in Gaussian98 Part I. The calculation of energies, gradients, vibrational frequencies and electric field derivatives, J. Mol. Struct. (THEOCHEM) 1–21 (1999) 461–462.
[55] T. Vreven, K.S. Byun, I. Komaromi, S. Dapprich, J.A. Montgomery, K. Morokuma, M.J. Frisch, Combining quantum mechanics methods with molecular mechanics methods in ONIOM, J. Chem. Theory Comput. 2 (2006) 815–826.
[56] M.J. Frisch, G.W. Trucks, H.B. Schlegel, G.E. Scuseria, M.A. Robb, J.R. Cheeseman, G. Scalmani, V. Barone, B. Mennucci, G.A. Petersson, H. Nakatsuji, M. Caricato, X. Li, H.P. Hratchian, A.F. Izmaylov, J. Bloino, G. Zheng, J.L. Sonnenberg, M. Hada, M. Ehara, K. Toyota, R. Fukuda, J. Hasegawa, M. Ishida, T. Nakajima, Y. Honda, O. Kitao, H. Nakai, T. Vreven, J.A. Montgomery Jr., J.E. Peralta, F. Ogliaro, M. Bearpark, J.J. Heyd, E. Brothers, K.N. Kudin, V.N. Staroverov, R. Kobayashi, J. Normand, K. Raghavachari, A. Rendell, J.C. Burant, S.S. Iyengar, J. Tomasi, M. Cossi, N. Rega, J.M. Millam, M. Klene, J.E. Knox, J.B. Cross, V. Bakken, C. Adamo, J. Jaramillo, R. Gomperts, R.E. Stratmann, O. Yazyev, A.J. Austin, R. Cammi, C. Pomelli, J.W. Ochterski, R.L. Martin, K. Morokuma, V.G. Zakrzewski, G.A. Voth, P. Salvador, J.J. Dannenberg, S. Dapprich, A.D. Daniels, Ö. Farkas, J.B. Foresman, J.V. Ortiz, J. Cioslowski, D.J. Fox, Gaussian 09, revision C 01, Gaussian, Inc., Wallingford CT, 2009.
[57] S. Shaik, D. Kumar, S.P. de Visser, A. Altun, W. Thiel, Theoretical perspective on the structure and mechanism of cytochrome P450 enzymes, Chem. Rev. 105 (6) (2005) 2279–2328.
[58] M. Reiher, O. Salomon, B. Artur Hess, Reparameterization of hybrid functionals based on energy differences of states of different multiplicity, Theor. Chem. Acc. 107 (1) (2001) 48–55.
[59] V.R.I. Kaila, G. Hummer, Energetics of direct and water-mediated proton-coupled electron transfer, J. Am. Chem. Soc. 133 (47) (2011) 19040–19043.
[60] M.-T. Zhang, L. Hammarström, Proton-coupled electron transfer from tryptophan: a concerted mechanism with water as proton acceptor, J. Am. Chem. Soc. 133 (23) (2011) 8806–8809.
[61] R. Latifi, M.A. Sainna, E.V. Rybak-Akimova, S.P. de Visser, Does hydrogen-bonding donation to manganese(IV)–oxo and iron(IV)–oxo oxidants affect the oxygen-atom transfer ability? A computational study, Chem. Eur. J. 19 (12) (2013) 4058–4068.